Energy Technology, Generation, Coversion, Storage, Distribution, Volume 4, Issue 10, 2016, pp. 1171–1178.
DOI: 10.1002/ente.201600028

Cyclic oxygen release characteristics of bi-functional CuO/CaO composite

Lunbo Duan*[a,b], Danilo Godino[c], Vasilije Manovic[b], Fabio Montagnaro[d], Edward J Anthony[b]

Abstract: Integrated Ca-Cu looping is a novel carbon capture technology which uses CuO to transport oxygen and CaO to capture CO_2 in the same process. Investigation on the oxygen release behavior of the bi-functional CuO/CaO composite is critical to assess the potential for applying this technology to solid fuels like coal. In this study, three different CuO/CaO composites having different relative percentages (CuO75CaO25, CuO50CaO50 and CuO25CaO75) were manufactured in a commercial granulator and then tested in a bubbling fluidized bed reactor to examine their oxygen release characteristics at temperatures in the 880–940°C range. All the composites exhibited clear oxygen release properties during the testing, indicating that the solid fuel can be directly oxidized rather than being gasified first in the Ca-Cu looping process. At the same temperature, the oxygen release rate of CuO25CaO75 is the fastest and its final oxygen yield is the largest, followed by CuO75CuO25 and CuO50CaO50. XRD results show that Ca_2CuO_3 is formed in the used samples of CuO75CuO25 and CuO50CaO50, but not in the case of CuO25CaO75, which may explain the performance difference observed. Further examination of the attrition and agglomeration behavior shows that all the composites are very stable and strong, and it appears that CuO25CaO75 is the most stable and strongest of the materials examined.

Introduction

Chemical looping combustion (CLC) holds the potential to economically produce power and other products like H_2 with inherent CO_2 separation [1-3]. A wide range of oxygen carriers has been proposed and tested by numerous researchers, as summarized elsewhere [1,2]. In recent years a new process, integrated chemical looping combustion and calcium looping combustion, has been proposed [4-12]. In this process, the use of CuO/CaO composite was suggested to provide two functions: transporting oxygen and capturing CO_2. Abanades et al. [4] proposed a process employing combined Ca and Cu chemical looping to produce H_2 and capture CO_2, as shown in Scheme 1. They then developed a conceptual design for this process [5]. As they noted, when oxidizing the CuO in the presence of $CaCO_3$, the prevention of $CaCO_3$ decomposition will be favored by high-pressure, low-temperature operation. For the calcination of $CaCO_3$ and the reduction of CuO with a fuel gas, syngas with a high CO content which can yield the highest reduction reaction enthalpies was required in order to obtain most or all of the heat necessary for calcination.

[Insert Scheme 1 here]
Scheme 1. CO_2 capture and H_2 production process proposed by Abanades et al. [4].

Manovic and Anthony [6] experimentally tested the composite containing CaO and CuO together with the addition of calcium aluminate cement as a binder in a thermogravimetric analyzer (TGA) by performing a number of calcination/reduction/oxidation/carbonation cycles and proposed several schemes for integrated Ca-Cu looping cycles. They also compared the capacity of different oxygen carriers as well as different CaO/CuO mixing structures [7, 8]. Kierzkowska and Muller [9] experimentally demonstrated the feasibility of this process by using a CaO-based and CuO-functionalized material without any support material which also showed high CO_2 uptake and oxygen carrying capacity over many cycles. Qin et al. [10] prepared and tested MgO-supported CaO/CuO composite in Ca-Cu looping cycles and achieved both good reactivity and composite stability. They further screened the thermal pre-treatment and operation conditions and found both thermal pre-treatment of CuO and steam addition were very effective in enhancing the cyclic reactivity of the composite sorbents [11]. Their recent study [12] also showed that the reduction of CuO was completed extremely quickly and the addition of steam was helpful in achieving matching kinetics for the two reactions.
At present, most studies focus on developing the process, preparing the composites and testing the reactivity of the materials, particularly the carbonation reactivity. Little research has been done on the effect of the composite on the CuO reactivity since CuO is considered to be very reactive. Furthermore, all the studies until now use gas (CH_4, CO and H_2) as fuel, which will be more expensive to deploy as a fuel than solid fuels such as coal. However, as it is well established, CuO has the ability to release oxygen as shown in reaction (1) and supply it to the solid fuel this can switch the first fuel conversion step from gasification in the normal CLC process to direct combustion in the chemical looping with oxygen uncoupling (CLOU) process [13-18]:

$$4CuO \rightarrow 2Cu_2O + O_2 \quad (1)$$

In this paper, the CuO/CaO composite was prepared in a commercial granulator to demonstrate the feasibility of scaling up of the method. Then the cyclic oxygen release performance was tested in a fluidized bed reactor and the assessment of the attrition/agglomeration behavior during oxygen release/oxidation cycles was also carried out.

Results and Discussion

Oxygen release behavior during cyclic tests

[a] Key Laboratory of Energy Thermal Conversion and Control, Ministry of Education, School of Energy and Environment, Southeast University, Nanjing, 210096, China;
[b] Centre for Combustion and CCS, School of Energy, Environment and Agrifood, Cranfield University, Cranfield, Bedfordshire MK43 0AL, UK; 3.
[c] Department of Chemical, Materials and Industrial Production Engineering, University of Naples Federico II, 80125 Napoli, Italy;
[d] Department of Chemical Sciences, University of Naples Federico II, 80126 Napoli, Italy.

This is the pre-peer reviewed version of the following article: L. Duan, D. Godino, V. Manovic, F. Montagnaro, E. J. Anthony, *Energy Technol.* **2016**, *4*, 1171, which has been published in final form at 10.1002/ente.201600028.
Published by Wiley. This is the Author Accepted Manuscript issued with: Creative Commons Attribution Non-Commercial License (CC:BY:NC 4.0).
The final published version (version of record) is available online at DOI:10.1002/ente.201600028. Please refer to Wiley Terms and Conditions for Self-Archiving.

Figure 1 shows the oxygen concentration/time profiles during the 1st, 5th and 10th cycle under inert atmosphere for all three samples at 940°C. Profiles with sand as the reference case are also included for comparison ("empty" case). As the oxidizing gas was switched to inert gas, oxygen volume (percentage) in the exit gas rapidly dropped to a given level and then stabilized to what can be regarded as a steady state level, except for the CuO25CaO75 case, where this value continued to drop albeit slowly and only slightly. The process consisted of a combination of two steps: i) vessel purging by N_2 when the oxygen percentage dropped rapidly and once the oxygen percentage dropped to a given level, oxygen release occurred, but there was still some oxygen left from the oxidizing stage; and ii) after about 10-20 s (which can be deduced from the sand test), the remaining oxygen is completely purged out of the system and further oxygen originates only from the decomposition of CuO. The stabilized value was clearly above that observed in the sand case confirming the occurrence of oxygen release. For each sample, the oxygen release/time profiles during different numbers of cycles overlapped each other and there was no observable decay within the tested time period, indicating the oxygen release properties were quite stable for all the samples.

[Insert Figure 1 here]

Figure 1. Oxygen release/time profiles over different cycles carried out at 940°C using the three different CuO/CaO composites. "Empty" refers to the reference case using sand

The oxygen release profiles for all samples at different temperatures are shown in Figure 2. At 880ºC, there was a slight oxygen release for all the composites. As the temperature increased, this release became more and more apparent. Over the tested period (360s), there was no clear oxygen concentration degradation observed for the CuO50CaO50 and CuO75CaO25 case, since there was enough oxygen available. At 920ºC and 940ºC, the oxygen volume (percentage) in the exit gas stream for the CuO25CaO75 case dropped gradually due to the limited oxygen carried present in this sample. Very interestingly, the oxygen percentage in the CuO25CaO75 case was always higher than in the other cases at the initial oxygen release stage for all temperatures.

[Insert Figure 2 here]

Figure 2. Oxygen release/time profiles for tests carried out at different temperatures and using the three different CuO/CaO composites. "Sand" refers to the reference case

Steady-state oxygen concentration and oxygen yield

In terms of the steady-state oxygen concentration during the test, it increased as the temperature increased for all three composites, as shown in Figure 3. The value was much lower than the theoretical equilibrium oxygen concentration. This phenomenon was also observed by Arjmand et al. [16] when they tested their $MgAl_2O_4$-supported CuO with a weight ratio of 40/60. The gas flow in our study diluted the oxygen concentration around the oxygen carrier particles very quickly and caused a relatively low steady-state oxygen concentration.

[Insert Figure 3 here]

Figure 3. Steady-state oxygen concentration vs. temperature

Equation 2 was used to assess the CuO conversion ratio during the oxygen release process:

$$Y = \frac{4M_{CuO} * n_{tot,in}}{m_{OC} * \alpha_{CuO}} \int_{t_0}^{t} \frac{x_{o2,OUT}}{1-x_{o2,OUT}} dt \quad (2)$$

where the oxygen yield Y is the ratio of produced oxygen taken up over the total oxygen that can be released from the CuO in an inert atmosphere; M_{CuO} is the molecular weight of CuO, g/mol; $n_{tot,in}$ is the total molar flow of gas entering the reactor, mol/s; m_{OC} is the mass of the oxygen carrier sample, g; α_{CuO} is the mass fraction of CuO in the sample; $x_{O2,OUT}$ is the percentage of oxygen leaving the reactor; and t_0 and t denote the initial and the end time of a generic inert phase, respectively. Therefore, if Y=1, this means the CuO is totally reduced to Cu_2O. Figure 4 shows the CuO conversion ratio as the time proceeds under an inert atmosphere. For CuO75CaO25, the oxygen yield increased almost linearly with time at all temperatures tested, indicating the oxygen release rate was quite stable and continuous. Higher temperatures promoted the total oxygen yield and at 940ºC, the final oxygen yield was 0.27 over the test. The oxygen yield profiles of CuO50CaO50 were similar to those of CuO75CaO25, but with a relatively lower value. There was trivial oxygen release at temperatures below 920ºC. For CuO25CaO75, Y fits almost linearly with time at 880ºC, 900ºC and 920ºC, similarly to the CuO75CaO25 case. At 940ºC, there were two obvious stages of oxygen release: a fast stage and a slow stage. The fast stage occurred before 150 s, and oxygen release was rapid and the yield was almost linear with time. The second stage began from 150 s, and at this stage, the oxygen release rate became slower than in the first stage. This is perhaps due to the mass transfer limitation since less oxygen was available from the parent crystal when Y>0.5. The final oxygen yield of CuO25CaO75 was 0.76 at 940ºC. During the tested period of 360 s, complete oxygen release did not occur for any of the composites. However, when nitrogen was used to simulate the oxygen release condition, reaction (1) could approach its equilibrium oxygen concentration, thus releasing oxygen at a limited rate, which may be slower than the actual rate in a real process, where the released oxygen would be immediately consumed by the fuel [16]. Thus, such an experimental approach would not readily yield the relevant rate of oxygen release since CuO decomposition is hindered by the high concentration of oxygen in the atmosphere surrounding the particles [16].

[Insert Figure 4 here]

Figure 4 Oxygen yield Y during the oxygen release period, for tests carried out at different temperatures and using the three different CuO/CaO composites.

In order to further explain why the CuO25CaO75 carrier exhibited the largest oxygen release rate and oxygen yield, scanning electron microscopy (SEM) and X-ray diffraction (XRD) analyses were carried out to examine the morphology and composition of the reacted composites. Figure 5 shows the

surface image of the reacted particles. It appears that CuO25CaO75 was the most porous and the surface of CuO50CaO50 was least porous. The solid surface of CuO50CaO50 perhaps blocked the diffusion of released oxygen outside the matrix. From the XRD results shown in Figure 6 it can be seen that, in the case of the cycled CuO75CaO25 and CuO50CaO50 samples, a new crystalline phase of Ca_2CuO_3 was found, probably due to the interaction [13] between copper oxide and calcium oxide during fluidization at high temperatures. The presence of Ca_2CuO_3 (absent in the CuO25CaO75 case) may explain why these samples were not able to release sufficient oxygen in the tests. On one hand, the production of Ca_2CuO_3 consumed CuO and reduced the available CuO. On the other hand, the Ca_2CuO_3 which may have a larger specific molar volume might block the passage of oxygen leaving the matrix. But the reason that CuO50CaO50 sample exhibited the poorest oxygen release performance still needs further exploration.

[Insert Figure 5 here]

Figure 5. SEM photos of the reacted particles of oxygen carriers

[Insert Figure 6 here]

Figure 6. XRD spectra of the reacted particles of oxygen carriers

Assessment of attrition and agglomeration

The elutriation rate was measured by calculating the mass of particles in the riser derived from the pressure drop in the reactor during the inert/oxidation cycles. Thus an elutriation rate was obtained in terms of the percentage of weight lost over time. The fines captured in the downstream filter were collected and weighed to help in calibrating the calculated value. The results are shown in Figure 7. As can be seen, the elutriation rate was usually high at the beginning of the experiment, probably due to the initial rounding effects on the surface asperities of the particles and the initial thermal shock [19]. Later on, the elutriation rate decreased rapidly. In general, the composites showed a low elutriation rate that changed a little after 4 h, reaching values close to zero for both CuO25CaO75 and CuO50CaO50, while an elutriation rate of 0.078%/h was reached for CuO75CaO25. It can also be observed in Figure 7 that the samples CuO75CaO25 and CuO25CaO75 showed the highest and the lowest elutriation rates, respectively. This was expected since a higher support (CaO) content normally brings a higher mechanical strength.

[Insert Figure 7 here]

Figure 7. Elutriation rates of the three samples

The particle size distribution (PSD) was next analyzed to assess the agglomeration potential of the particles. As shown in Figure 8, by comparing the PSDs before and after the cyclic tests, only a small amount of large particles, coarser than the original ones, was produced for CuO25CaO75, while a slightly higher amount was produced for CuO50CaO50 and CuO75CaO25 composites. As the CuO content increased in the composites, the coarse particles in the cycled material increased. This is because CuO particles melt more easily and stick together to produce coarse particles than CaO particles. However, in this work, the agglomeration was trivial for all particles, which was also verified by the SEM pictures.

[Insert Figure 8 here]

Figure 8. Particle size distribution of the reacted particles of oxygen carriers

Table 1. Composition of the raw limestone

Component	(wt.%)
Al_2O_3	0.082
BaO	0.007
CaO	53.9
Fe_2O_3	0.015
K_2O	0.007
MgO	0.185
MnO_2	0.008
Na_2O	0.053
P_2O_5	0.007
SO_3	0.034
SiO_2	0.701
SrO	0.017
TiO_2	0.006
LOI	44.98

Table 2. Composition of the coarse CuO

Component	Acceptance level (wt.%)
Total Copper content as Cu	>78.0%
Cupric Oxide as CuO	>97.5%
Cuprous Oxide as Cu_2O	<0.1%
Iron as Fe	<0.025%
Nickel	<0.035%
Chloride as Cl	<0.03%
Calcium as Ca	<0.03%
Sulphate as SO_4	<0.03%
Moisture as free H_2O	<0.2%

Table 3. Characterization of the particles

Samples	CuO75CaO25	CuO50CaO50	CuO25CaO75
Bulk density / $kg \cdot m^{-3}$	1700	1410	1330
Crushing strength / N	1.31	1.50	1.63
Crystalline phases identified by	$Ca(OH)_2$, CuO, $CaCO_3$*	$Ca(OH)_2$, CuO, $CaCO_3$*	$Ca(OH)_2$, CuO, $CaCO_3$*

XRD	

*: minor phase

Conclusions

Three different bi-functional CuO/CaO composites were manufactured in a commercial granulator and their cyclic oxygen release performance was examined in a fluidized bed reactor; results showed that:

1) Clear oxygen release took place at test temperatures from 880ºC to 920ºC for all the samples and the oxygen release performance did not decay within the number of cycles tested.

2) Steady-state oxygen concentration increased with the temperature.

3) The oxygen yields of CuO75CaO25 and CuO50CaO50 were lower than that of CuO25CaO75, probably due to formation of the interaction product Ca_2CuO_3.

4) No serious agglomeration and attrition occurred.

Experimental Section

Preparation of the composite

To demonstrate the feasibility of scaling up the CuO/CaO composite preparation methods, CaO powder was derived from raw limestone (its composition is shown in Table 1) after calcination in a muffle furnace at 900°C for 14 h. The particle size distribution of the obtained powder showed that d(0.1) = 28.86 µm, d(0.2) = 52.86 µm, d(0.5) = 126.84 µm, and d(0.9) = 430.19 µm. CuO powder was obtained by grinding coarse CuO powder (its composition is shown in Table 2) in an Orto-Alesa ball mill drum (15 L capacity) and the particle size distribution of the obtained powder showed that d(0.1) = 21.78 µm, d(0.2) = 30.19 µm, d(0.5) = 51.80 µm, and d(0.9) = 116.94 µm. The composites were produced with a mechanical granulator (Glatt GmbH, Switzerland). A controlled amount of water was sprayed intermittently during granulation with a nozzle, which produced micrometre-sized water droplets (<300 µm) which acted as binder. The water droplet size and the total amount of water added appeared to be the most crucial factors affecting the size of the composites based on the experience gained after long-time operation. The pellet size was also controlled by the speed of a pair of rotor blades attached to the vessel, one agitator on the bottom and one chopper on the side. Typically, one batch of pellets could be produced in 15–20 min. After granulation, the pellets were dried at 200°C in an oven for 2 h and sieved through stainless steel screens to obtain particles in the size range of 355–425 µm. After each run, the particles beyond this range were recycled into the granulator, so almost no waste material was produced during the operation, which ensured an efficient utilization of the material.

Three types of pellets were prepared with different mass ratios of CuO and CaO, labelled as: i) CuO75CaO25 (75% CuO and 25% CaO), ii) CuO50CaO50 (50% CuO and 50% CaO) and iii) CuO25CaO75 (25% CuO and 75% CaO). The forms of the copper and calcium in the composite were determined by an X-ray diffraction (XRD) analyzer (Bruker D5005 Diffractometer, USA). The bulk density was measured with a graduated cylinder and the crushing strength was characterized by a digital force gauge (SHIMPO FGE-5XY, Japan). The results of the characterization are summarized in Table 3. It is obvious that as the CuO fraction in the composite increased, the bulk density increased, while as the CaO fraction increased, the crushing strength increased. According to XRD analysis, CuO and $Ca(OH)_2$ are the main crystalline components in the composite together with minor amounts of $CaCO_3$.

Experimental Details

Fluidized bed test

The experiments were performed in a bench-scale fluidized bed system, which consisted of a gas feeding system, bubbling fluidized bed reactor, metallic filter and gas analyzer unit, as shown in Figure 9. The major components of the fluidized bed reactor consisted of a quartz tube riser of 32 mm inner diameter and 550 mm height, and an outer stainless steel tube (37 mm inner diameter and 1180 mm height). A sintered plate was placed on the bottom of the quartz tube, which acted as gas distributor with a pre-heater section at the base to achieve the desired temperature. The entire system was placed inside an electrically-heated furnace. A particle filter with 60 µm filter element was placed at the top of the apparatus, in order to recover solids elutriated from the reactor. The flow rates of different gases were controlled using accurate Mass Flow Controllers (Bronkhorst, Netherlands). After drying, the exit gas stream was directly sampled by the analyzer (ADC MGA-300, UK), pre-calibrated for low oxygen percentage use. A PICO Data Acquisition System (PICO Technology, UK) was employed to record all flowrates, temperature, pressure and gas concentration data over the entire test.

[Insert Figure 9 here]
Figure 9. Bench-scale fluidized bed system

16 g of oxygen carrier particles with 355–425 µm size range was initially loaded into the reactor, and then the reactor was heated to 880°C under 5% O_2/95% N_2 atmosphere to ensure full oxidation of the samples. Then, the atmosphere was shifted between pure N_2 and 5% O_2/95% N_2 to achieve the oxygen release/oxidation cycles. After 10 cycles, the temperature was increased to 900°C in 5% O_2/95% N_2 atmosphere and then another 10 cycles were carried out at 900°C. Following the same procedure, tests at 920°C and 940°C were also performed. Basically, 10 inert/oxidation cycles at four temperature levels (880°C, 900°C, 920°C and 940°C) were achieved for each composite in this study. A total gas flowrate of 3 L/min was supplied to the system during the entire test to achieve a fluidization velocity in the reactor higher than 0.2 m/s, which is approximately 3 times the minimum fluidization velocity of the composites, thus ensuring a vigorously fluidized bed.

Acknowledgements

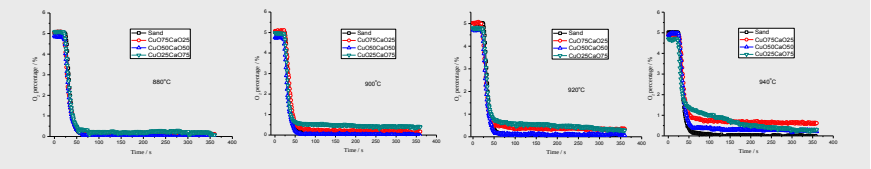
Financial supports from the NSFC (51206023) and UKCCSRC are acknowledged. The authors are grateful to Prof. Piero Salatino (University of Naples) for useful discussion. The support of the Erasmus Project funding for the stay at Cranfield University of one of the authors (DG) is gratefully acknowledged.

Keywords: integrated Ca-Cu looping • oxygen release • steady-state oxygen concentration • attrition • agglomeration

[1] J. Adanez, A. Abad, F. Garcia-Labiano, P. Gayan, L. F. de Diego, *Prog. Energy Combust. Sci.* **2012**, *38*, 215-282.
[2] B. Moghtaderi, *Energy Fuels* **2012**, *26*, 15-40.
[3] A. Lyngfelt, *Appl. Energy* **2014**, *113*, 1869-1873.
[4] J. C. Abanades, R. Murillo, J. R. Fernandez, G. Grasa, I. Martínez, *Environ. Sci. Technol.* **2010**, *44*, 6901-6904.
[5] J. R. Fernández, J. C. Abanades, R. Murillo, G. Grasa, *Int. J. Greenhouse Gas Control* **2012**, *6*, 126-141.
[6] V. Manovic, E. J. Anthony, *Environ. Sci. Technol.* **2011**, *45*, 10750-10756.
[7] V. Manovic, E. J. Anthony, *Energy Fuels* **2011**, *25*, 4846-4853.
[8] V. Manovic, Y. Wu, I. He, E. J. Anthony, *Ind. Eng. Chem. Res.* **2011**, *50*, 12384-12391.
[9] A. M. Kierzkowska, C. R. Mueller, *Energy Environ. Sci.* **2012**, *5*, 6061-6065.
[10] C. Qin, J. Yin, W. Liu, H. An, B. Feng, *Ind. Eng. Chem. Res.* **2012**, *51*, 12274-12281.
[11] C. Qin, J. Yin, C. Luo, H. An, W. Liu, B. Feng, *Chem. Eng. J.* **2013**, *228*, 75-86.
[12] C. Qin, B. Feng, J. Yin, J. Ran, L. Zhang, V. Manovic，*Chem. Eng. J.* **2015**, *262*, 665-675.
[13] F. Donat, W. Hu, S. A. Scott, J. S. Dennis, *Ind. Eng. Chem. Res.* **2015**, *54*, 6713-6723.
[14] T. Mattisson, A. Lyngfelt, H. Leion, *Int. J. Greenhouse Gas Control* **2009**, *3*, 11-19.
[15] P. Gayán, I. Adánez-Rubio, A. Abad, L. F. de Diego, F. García-Labiano, J. Adánez, *Fuel* **2012**, *96*, 226-238.
[16] M. Arjmand, M. Keller, H. Leion, T. Mattisson, A. Lyngfelt, *Energy Fuels* **2012**, *26*, 6528-6539.
[17] L. Xu, J. Wang, Z. Li, N. Cai, *Energy Fuels* **2013**, *27*, 1522-1530.
[18] B. Wang, H. Zhao, Y. Zheng, Z. Liu, R. Yan, C. Zheng, *Fuel Process. Technol.* **2012**, *96*, 104-115.
[19] F. Scala, F. Montagnaro, P. Salatino, *Energy Fuels* **2007**, *21*, 2566-2572.

Entry for the Table of Contents (Please choose one layout)

FULL PAPER

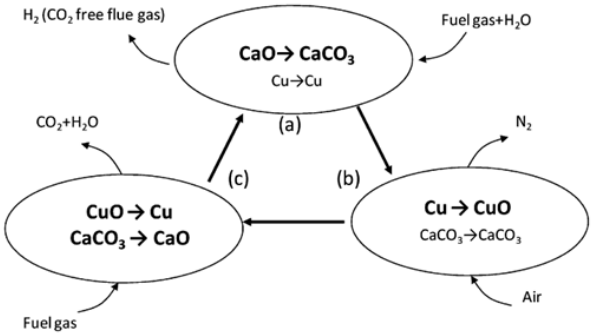


Clear and stable oxygen release occurred for all the tested CuO/CaO composites at temperatures in the 880–920 ºC range. The steady-state oxygen concentration increased with the temperature. CuO25CaO75 showed the highest oxygen concentration and final oxygen yield.

Lunbo Duan, Danilo Godino, Vasilije Manovic, Fabio Montagnaro, Edward J Anthony*

Page No. – Page No.

Cyclic oxygen release characteristics of bi-functional CuO/CaO composite



Scheme 1. CO_2 capture and H_2 production following the process proposed by Abanades et al. [4].

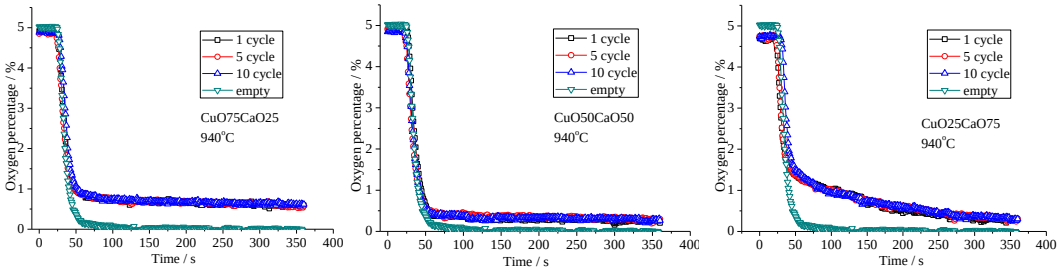


Figure 1. Oxygen release/time profiles over different cycles carried out at 940°C using the three different CuO/CaO composites. "Empty" refers to the reference case using sand

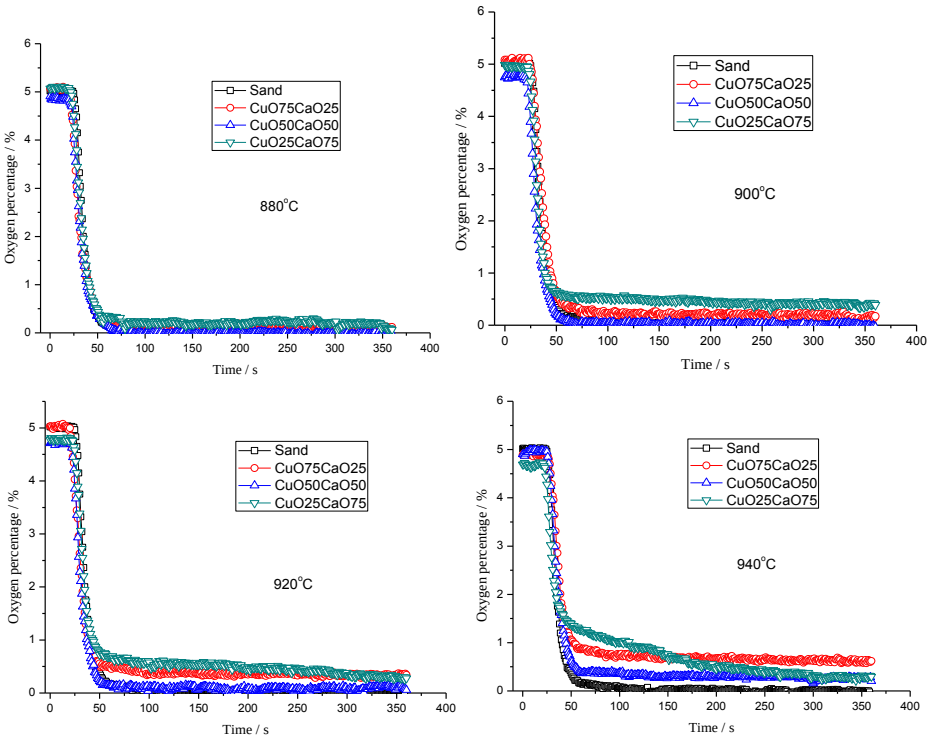


Figure 2. Oxygen release/time profiles for tests carried out at different temperatures and using the three different CuO/CaO composites. “Sand” refers to the reference case

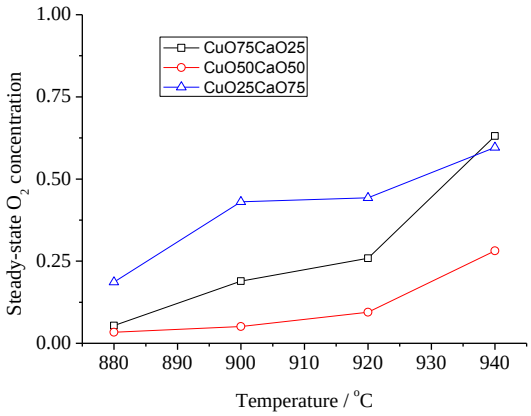


Figure 3. Steady-state oxygen concentration vs. temperature

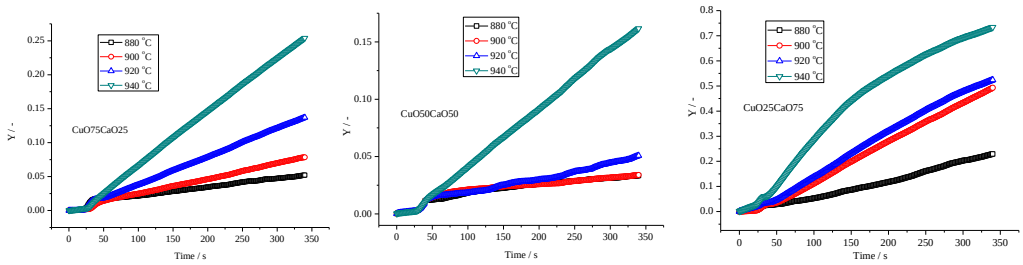
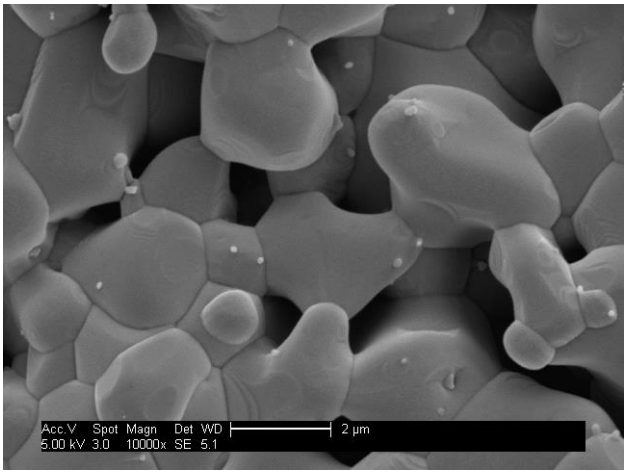
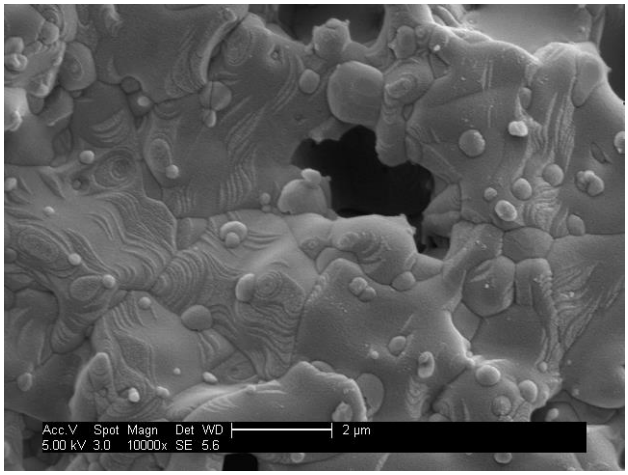


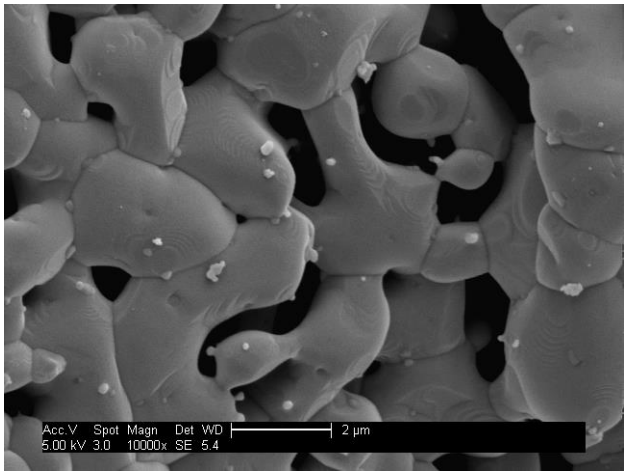
Figure 4 Oxygen yield Y during the oxygen release period, for tests carried out at different temperatures and using the three different CuO/CaO composites.



CuO75CaO25

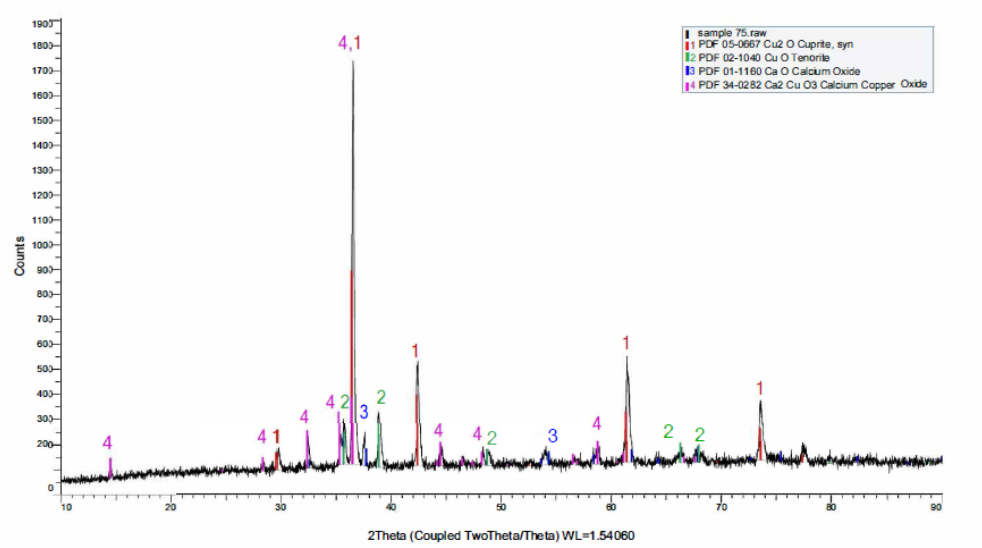


CuO50CaO50

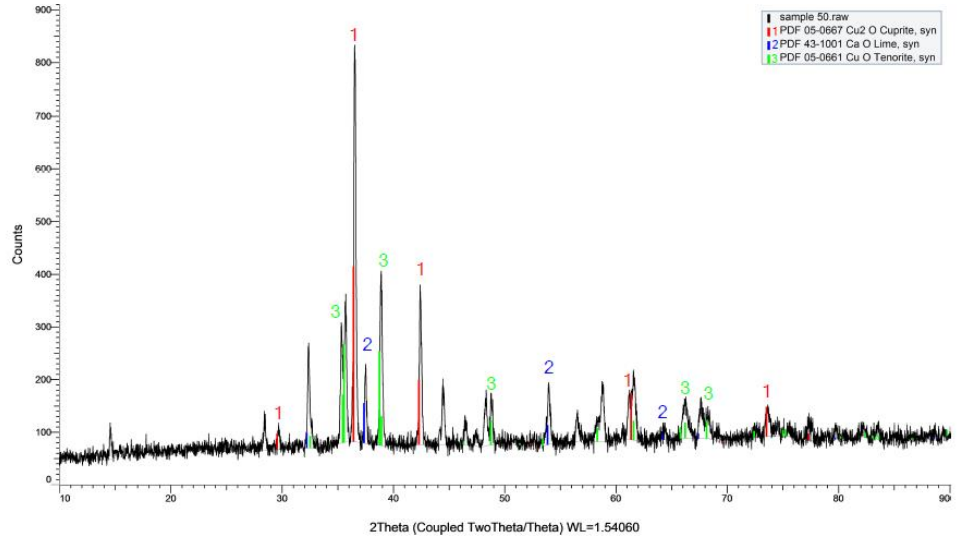


CuO25CaO75

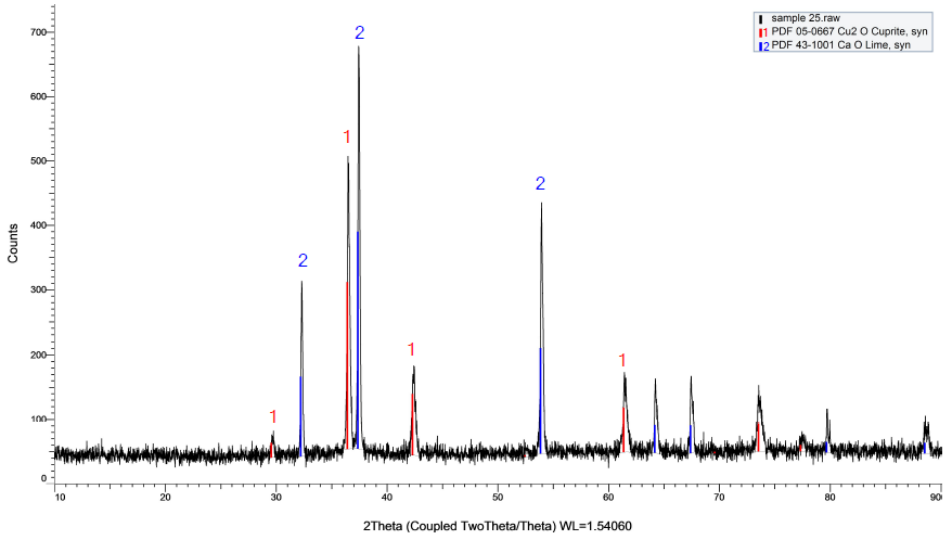
Figure 5. SEM photos of the reacted particles of oxygen carriers



CuO75CaO25



CuO50CaO50



CuO25CaO75

Figure 6. XRD spectra of the reacted particles of oxygen carriers

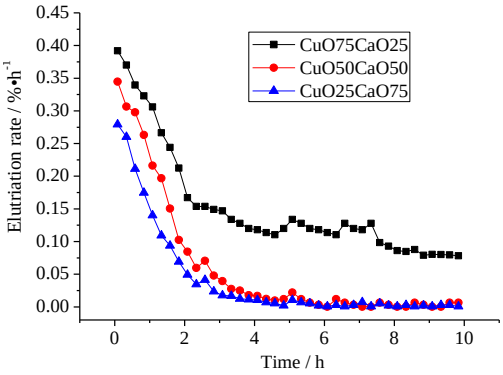


Figure 7. Elutriation rates of the three samples

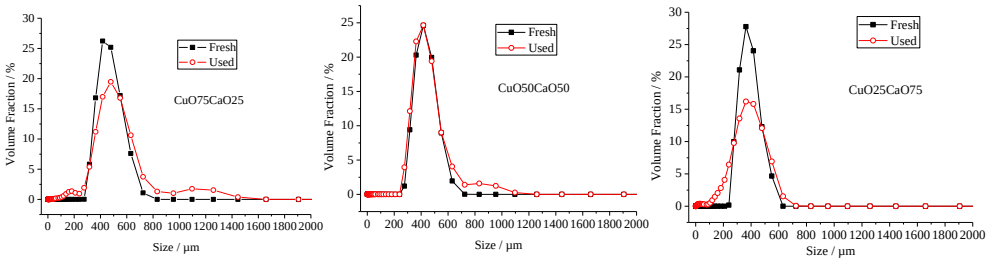


Figure 8. Particle size distribution of the reacted particles of oxygen carriers

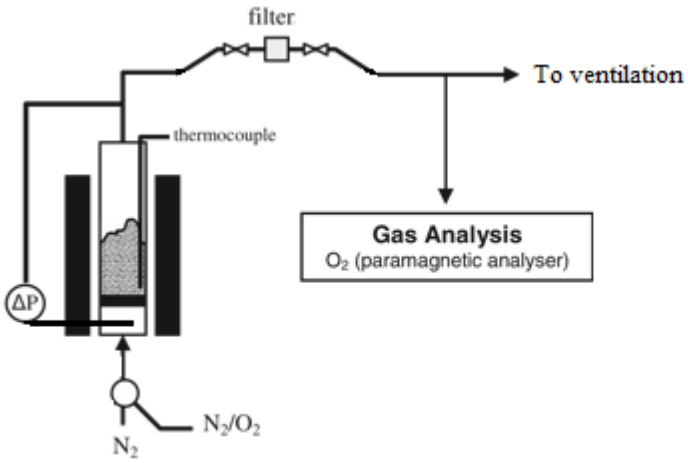


Figure 9. Bench-scale fluidized bed system



https://dspace.org/

Cyclic oxygen release characteristics of bifunctional copper oxide/calcium oxide composites

Duan, Lunbo; Godino, D.; Manovic, Vasilije; Montagnaro, F.; Anthony, Edward J.

2016-10-12
Wiley
http://dx.doi.org/10.1002/ente.201600028
L. Duan, D. Godino, V. Manovic, F. Montagnaro, E. J. Anthony, Cyclic oxygen release characteristics of bifunctional copper oxide/calcium oxide composites. Energy Technology, Volume 4, Issue 10, 2016, pp.1171-1178

Downloaded from a DSpace repository. https://dspace.org/